

ARMY RESEARCH LABORATORY



Modeling and Simulation of Nonlinear Transmission Lines

by Frank Crowne

ARL-TR-5062

January 2010

NOTICES

Disclaimers

The findings in this report are not to be construed as an official Department of the Army position unless so designated by other authorized documents.

Citation of manufacturer's or trade names does not constitute an official endorsement or approval of the use thereof.

Destroy this report when it is no longer needed. Do not return it to the originator.

Army Research Laboratory

Adelphi, MD 20783-1197

ARL-TR-5062

January 2010

Modeling and Simulation of Nonlinear Transmission Lines

Frank Crowne

Sensors and Electron Devices Directorate, ARL

REPORT DOCUMENTATION PAGE

Form Approved
OMB No. 0704-0188

Public reporting burden for this collection of information is estimated to average 1 hour per response, including the time for reviewing instructions, searching existing data sources, gathering and maintaining the data needed, and completing and reviewing the collection information. Send comments regarding this burden estimate or any other aspect of this collection of information, including suggestions for reducing the burden, to Department of Defense, Washington Headquarters Services, Directorate for Information Operations and Reports (0704-0188), 1215 Jefferson Davis Highway, Suite 1204, Arlington, VA 22202-4302. Respondents should be aware that notwithstanding any other provision of law, no person shall be subject to any penalty for failing to comply with a collection of information if it does not display a currently valid OMB control number.

PLEASE DO NOT RETURN YOUR FORM TO THE ABOVE ADDRESS.

1. REPORT DATE (DD-MM-YYYY) January 2010		2. REPORT TYPE Progress		3. DATES COVERED (From - To) June to October 2009	
4. TITLE AND SUBTITLE Modeling and Simulation of Nonlinear Transmission Lines				5a. CONTRACT NUMBER	
				5b. GRANT NUMBER	
				5c. PROGRAM ELEMENT NUMBER	
6. AUTHOR(S) Frank Crowne				5d. PROJECT NUMBER	
				5e. TASK NUMBER	
				5f. WORK UNIT NUMBER	
7. PERFORMING ORGANIZATION NAME(S) AND ADDRESS(ES) U.S. Army Research Laboratory ATTN: RDRL-SER-E 2800 Powder Mill Road Adelphi, MD 20783-1197				8. PERFORMING ORGANIZATION REPORT NUMBER ARL-TR-5062	
9. SPONSORING/MONITORING AGENCY NAME(S) AND ADDRESS(ES) U.S. Army ARDEC Picatinny Arsenal, NJ 07806-5000				10. SPONSOR/MONITOR'S ACRONYM(S)	
				11. SPONSOR/MONITOR'S REPORT NUMBER(S)	
12. DISTRIBUTION/AVAILABILITY STATEMENT Approved for public release; distribution unlimited.					
13. SUPPLEMENTARY NOTES					
14. ABSTRACT This technical report summarizes design work done for ARDEC Picatinny Arsenal from April to October 2009 as part of an effort to design and fabricate nonlinear transmission lines (NLTL) based on ferroelectric materials. These lines were intended to be key components in a compact source of high-power microwaves (HPM) that could be carried by artillery rounds and used to disrupt battlefield communications. The effort, which was begun in 2008, centered on implementing work previously done by General Atomics two decades ago. Although interrupted sporadically by changes in focus of the primary effort, the effort has progressed to a point where with proper resources it could be a valuable contribution to future HPM munitions. This TR incorporates five informal reports sent to ARDEC involving the modeling and simulation portion of the NLTL design effort, as requested by ARDEC. It will serve to document the resulting software products and to be a springboard for future design work.					
15. SUBJECT TERMS Nonlinear, soliton, HPM, transmission line, modeling					
16. SECURITY CLASSIFICATION OF:			17. LIMITATION OF ABSTRACT UU	18. NUMBER OF PAGES 40	19a. NAME OF RESPONSIBLE PERSON Frank Crowne
a. REPORT Unclassified	b. ABSTRACT Unclassified	c. THIS PAGE Unclassified			19b. TELEPHONE NUMBER (Include area code) (301) 394-5759

Contents

List of Figures	iv
1. Introduction: The Nonlinear Transmission Line	1
2. Selection of Capacitance-Voltage Dependence for NLTL Circuit	2
2.1 Ikezi's Model.....	3
2.2 Brown's Model.....	4
3. Nonlinear Circuit Software Development For Transmission Line	6
3.1 Brown and Ikezi Circuits.....	6
3.2 State Variables.....	7
3.3 The Method of Partial Charges	9
4. Determining the Resistive Losses in the NLTL BASED on Loss Tangents	10
5. Realistic Antenna Coupling Via an RC Circuit	16
6. Description of Mathematica Code	18
7. Results of Preliminary Simulations	20
8. Movies of NLTL Interior	23
9. Systems Issues	24
10. Conclusions	26
11. References	27
Appendix. Brown-Ikezi Network Equations	29
Distribution List	34

List of Figures

Figure 1. General discrete transmission-line circuit.	2
Figure 2. NLTL structure used for fabrication at ARL.....	2
Figure 3. The function $Q(V)$ evaluated from Brown’s fitting expression: red – multiplication, blue – integration.	5
Figure 4. Ikezi-Brown NLTL circuit.	6
Figure 5. Two-inductor circuit.	8
Figure 6. Series LRC circuit.	8
Figure 7. Placement of resistors in Brown-Ikezi NLTL circuit.	11
Figure 8. Loss tangent of a BST varactor vs. frequency at different temperatures without (a) and under 20 V dc bias (b). The dotted line represents the $\tan \delta \sim \omega^{1/3}$ power law.....	15
Figure 9. NLTL with simple resistive load.....	17
Figure 10. NLTL with RC circuit load to simulate antenna reactance.	17
Figure 11. Ikezi normalized short test pulse shape; time scale in NLTL low-frequency single-stage periods.....	20
Figure 12. Low voltage response to figure 11 test pulse at end of NLTL.	21
Figure 13. High voltage response to figure 11 test pulse at end of NLTL; note solitons.	21
Figure 14. Ikezi normalized long test pulse shape.....	22
Figure 15. Low voltage response to figure 14 test pulse at end of NLTL.	22
Figure 16. High voltage response to figure 14 test pulse at end of NLTL; note solitons.	23
Figure A-1. Brown-Ikezi NLTL circuit.	29

1. Introduction: The Nonlinear Transmission Line

Transmission lines are ubiquitous in almost all high-frequency RF circuits, where they replace the standard wire connections used for assembling circuits at lower frequencies. The many forms they take, involving complex geometries and exotic materials, are conditioned by the task of delivering RF energy from one circuit location to another. A less common use of transmission lines is as actual RF devices – switches, phase shifters, filters, etc. – which exploit their ability to perform various impedance functions and versatility with regard to fabrication. For example, varying lengths of the same transmission line can be used as capacitors, inductors, or delay lines for matching circuit subunits such as amplifiers (1). When used in this way, the transmission line is usually a linear circuit component. A considerably less common use of nonlinear transmission lines (NLTL) is for large-signal device design – phase shifters come to mind (2) – although some early work on distributed amplifiers could qualify as such (3).

The structure of a transmission line can be either continuous or discrete. Whereas continuous transmission lines are typically waveguide-based (3a), lines with discrete structure usually consist of repeated identical subcircuits made up of lumped elements. A useful definition of a NLTL is an ordinary transmission line whose electrical characteristics are functions of local voltages and currents. Thus, the prototypical discrete transmission line shown in figure 1 is made up of lumped elements – resistors, capacitors, inductors, etc. – any one of which can be voltage dependent. In the 1980's, NLTL were fabricated by inserting shunt diodes periodically into a transmission line to create nonlinearity in its overall electrical response (3b). Although these lines had very useful properties, they were never capable of much power handling due to the semiconductor nature of the diodes used. At the end of the 1980's, the Ikezi group at General Atomics (4) studied layered structures consisting of parallel-plate waveguides in which layers of ferroelectric material (specifically, barium strontium titanate, or BST) alternated with layers of simple dielectric (see figure 2); these structures now represent the canonical version of high-voltage NLTLs, and are often encountered in the NLTL literature to this day. Mark Litz and I were first made aware of the work of Ikezi's group in 2007, as a possible way to address the need of ARDEC for a HPM source, and it has been the basis for our effort at ARL ever since.

In this report I will describe my efforts to model the electromagnetic response of this type of transmission line numerically, as requested by ARDEC in the summer of 2009.

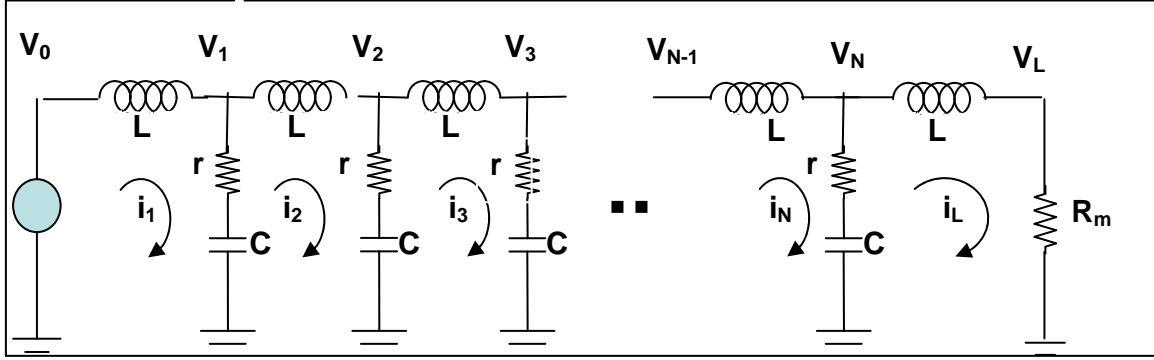


Figure 1. General discrete transmission-line circuit.

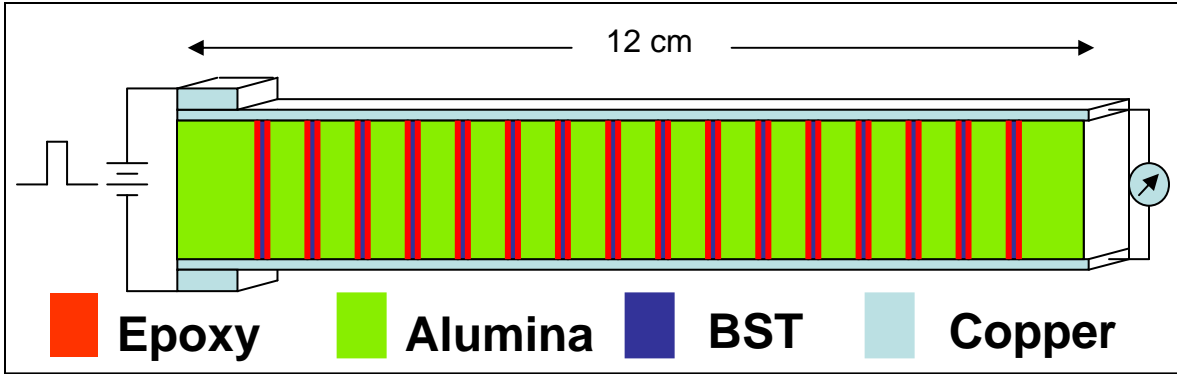


Figure 2. NLTL structure used for fabrication at ARL.

2. Selection of Capacitance-Voltage Dependence for NLTL Circuit

Much of the NLTL design work published in the literature is numerical in nature. The need to use numerical modeling to design a useful NLTL is regrettable in many ways, the most important of which is that easy-to-use design rules are seldom derivable from simulations. After much labor, Ikezi et al., at General Atomics (5) published an example of one such design rule for finding the frequency at which the power from a NLTL was a maximum. At ARL we used this rule extensively in our previous effort. The design rule was formulated by performing a series of numerical simulations of their NLTL circuit model for various line parameters, and extracting the peak power frequency by Fourier-transforming the computed time dependence of the power out of the line and looking for its peak value. Their results were published in the form of a curve, which they fitted to the empirical function

$$\frac{\omega}{\omega_b} = 1.5 \log_{10} \left(\frac{E}{E_0} \right) + 1.25$$

where ω is the peak-power frequency of the output soliton pulse train, ω_b is the width of the lowest NLTL pass band when treated as a linear (small-signal) transmission line, E is the electric field measured at the input of the NLTL, and E_0 is a scaling field of order 10 kV. Because the relationship implied by this formula between the small-signal and large-signal quantities is obscure, its usefulness for evaluating other systems is problematic. Because we were unable to make any accurate power measurements, we were unable to check how good the equation was; nevertheless, we were able to use the dependence on ω_b to design the NLTL at a prespecified frequency, using an additional equation taken from (6).

Because the nonlinear response of the NLTL is based on the voltage dependence of BST capacitors, it is vital that these components be modeled as precisely as possible. At this time we have two literature-based modeling functions, one the original choice of Ikezi in 1988 (5) and the other that of Martin Brown in his 1997 thesis (7). In this section I will explain why the former was preferred over the latter as a basis for this modeling work, and propose a third alternative with features of both.

2.1 Ikezi's Model

The model used by the Ikezi group for the voltage dependence of BST capacitors is based on a fundamental relationship between the electric displacement in BST and an external electric field, which they write as follows:

$$E = \frac{D}{\epsilon\epsilon_0} + \frac{D^3}{\epsilon^3\epsilon_0^3 E_0^2}$$

The quantity D gives the charge per unit area induced on the metal walls of the parallel-plate transmission line, and hence, can be multiplied by the area of contact A between the metal and a given ferroelectric layer to extract the charge per ferroelectric layer induced on the walls:

$$D = \frac{Q}{A} \Rightarrow Q = AD$$

while the electric field E equals the voltage V between the walls divided by the height of the guide:

$$E = \frac{V}{h} \Rightarrow V = Eh$$

Then together these quantities let us define a function $V(Q)$ which can be used to specify the capacitance of the line:

$$\begin{aligned}
V &= E_0 h \left[\frac{Q}{\epsilon \epsilon_0 E_0 A} + \left(\frac{Q}{\epsilon \epsilon_0 E_0 A} \right)^3 \right] \\
\Rightarrow 1 &= E_0 h \frac{d}{dV} \left[\frac{Q}{\epsilon \epsilon_0 E_0 A} + \left(\frac{Q}{\epsilon \epsilon_0 E_0 A} \right)^3 \right] = E_0 h \left[\frac{1}{\epsilon \epsilon_0 E_0 A} + \frac{3}{(\epsilon \epsilon_0 E_0 A)^3} Q^2 \right] \frac{dQ}{dV} \\
&= \frac{h}{\epsilon \epsilon_0 A} \left[1 + 3 \left(\frac{Q}{\epsilon \epsilon_0 E_0 A} \right)^2 \right] \frac{dQ}{dV} \\
\Rightarrow C(V) &= \frac{dQ}{dV} = \left[1 + 3 \left(\frac{Q(V)}{\epsilon \epsilon_0 E_0 A} \right)^2 \right]^{-1} \frac{\epsilon \epsilon_0 A}{h}
\end{aligned}$$

Note that in order to compute the capacitance, we must invert the function $V(Q)$ numerically.

The form of this expression, which is a consequence of the crystal physics of BST (8), predicts a capacitance versus voltage with the following properties:

1. At small voltages (small D) it predicts a constant capacitance of the usual form, i.e.,

$$C = \frac{\epsilon \epsilon_0 A}{h},$$

2. The capacitance is independent of polarity, and
3. For large voltages the capacitance decreases algebraically as $V^{-2/3}$.

It is worth noting that the expression used by Ikezi is clearly a truncation of an infinite series, and indeed, it is common practice with in most of the ferroelectrics literature to write

$$E = aD + bD^3 + cD^5$$

For our purposes, it is significant that this implies a falloff in the capacitance as $V^{-4/5}$ with voltage. The large- V behavior is thus ambiguous, and can only be resolved by fitting. Note that the procedure for fitting experimental data to polynomials is especially simple, a further advantage to using Ikezi's expressions.

2.2 Brown's Model

In contrast to the Ikezi physics-based model, the model used by Brown seems to be entirely *ad hoc*, and violates both the material constraints and the standard laws of electrostatics, casting his entire simulation effort into doubt:

- (1) He assumes that the relationship between charge and voltage is

$$Q = C(V)V$$

whereas in fact the correct relationship is

$$Q(V) = \int_0^V C(v) dv$$

(2) He postulates a diodelike functional dependence for $C(V)$ that depends on polarity:

$$C(V) = C_0 \left[\alpha + (1 - \alpha) e^{-V/V_c} \right]$$

In addition, this expression predicts a strong increase for negative V , which is unphysical.

It is interesting to determine the difference between Brown's expression and the correct expression for $Q(V)$: his simple multiplication gives

$$Q(V) = C(V)V = C_0 V \left[\alpha + (1 - \alpha) e^{-V/V_c} \right]$$

while the correct expression gives

$$Q(V) = C_0 \int_0^V \left[\alpha + (1 - \alpha) e^{-V/V_c} \right] dV = C_0 \left[\alpha V + (1 - \alpha) V_c \left\{ 1 - e^{-V/V_c} \right\} \right]$$

The plot shown in figure 3 illustrates the difference:

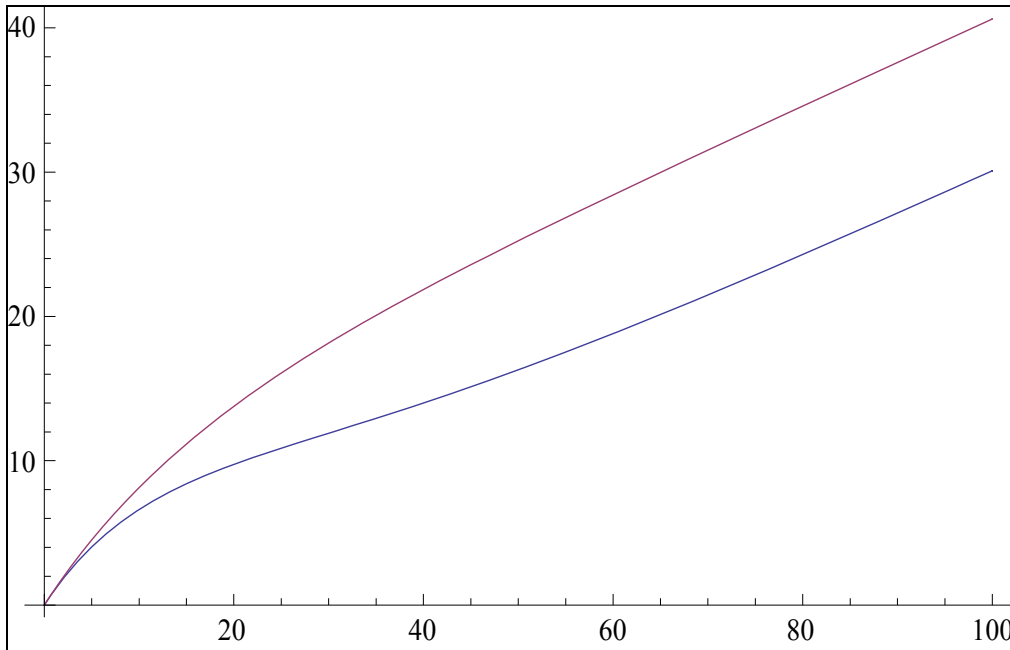


Figure 3. The function $Q(V)$ evaluated from Brown's fitting expression: red – multiplication, blue – integration.

Clearly the two functions are almost identical for small voltages, and differ only by an offset for large voltages; however, the severe change in slope at intermediate voltages will greatly distort the waveform of an ac signal as it passes through the intermediate voltage range.

These deficiencies persuade us to adopt the original Ikezi relations in our simulations.

3. Nonlinear Circuit Software Development For Transmission Line

Because of its flexibility and proven track record with regard to computational accuracy and speed, the mathematical package Mathematica™ has been chosen for software support of the NLTL design. In order to reduce the learning-curve burden for future users, code written for this package will be translated into MathCad™ in 2010 if funding permits; meanwhile, the basic analysis of the NLTL performance benefits greatly from the feasibility of writing transparent software that is easily changed and physically motivated, and is tailored to the specifics of the NLTL problem rather than relying on more broadly applicable circuit software such as PSPICE which cannot be “tuned” internally, i.e., lack of access to source code.

The approach to circuit modeling adopted here takes advantage of the simplicity of the NLTL circuit model which in turn is a consequence of the underlying parallel-plate waveguide geometry of the latter. A more complex propagation structure would require much more powerful mathematical methods to treat correctly. The modeling will be described in the following sections.

3.1 Brown and Ikezi Circuits

Both Brown and Ikezi adopt a simple series-parallel circuit model for the NLTL (see figure 4).

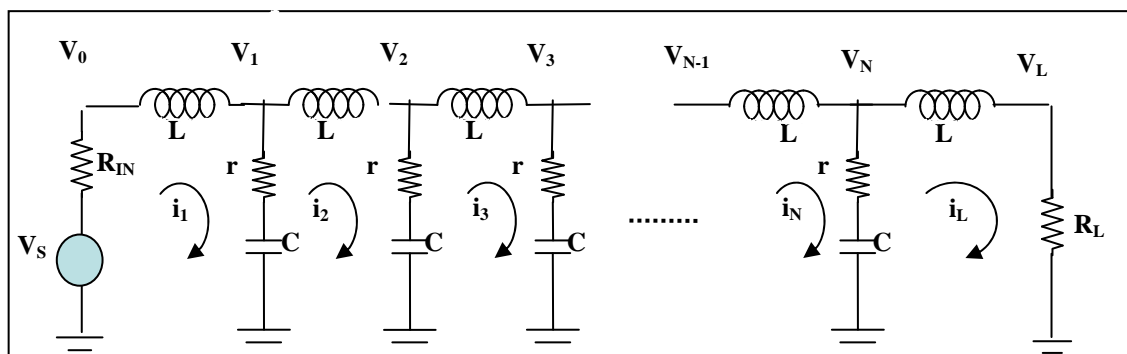


Figure 4. Ikezi-Brown NLTL circuit.

A justification of this circuit structure will be given in a future report. The original circuit analyzed at General Atomics had no resistances; the various resistors shown here were added by Brown. The circuit is an oversimplification of the real NLTL; roughly speaking, the inductors represent the alumina layers, while the shunt lines represent the BST layers. This

oversimplification will eventually be removed in our modeling effort. The capacitors C are taken to be nonlinear elements.

3.2 State Variables

Before the advent of circuit simulators, it was well understood that nonlinear circuits must be approached as individual problems. This is in contrast to linear circuits, which allow a universal approach to computations based on straightforward matrix computations. Textbooks on circuit theory routinely introduce the idea of the “state” of a circuit, by which they mean a list of all the currents flowing through the various circuit components and all the voltage drops across them. When these quantities depend on time, as in an ac circuit, their values are obtained from differential equations. For the special case of linear circuits driven by sinusoidal sources, these differential equations reduce to algebraic equations that can easily be solved by matrix methods. Transient excitation, e.g., by pulses, require the original differential equations and numerical methods, as do circuits with nonlinear elements.

It is important for numerical reasons that these differential equations all be *first-order* in time, i.e., if we describe the circuit state using a vector of currents and voltages $\vec{x} = (V_1, I_1, V_2, I_2, V_3, I_3, \dots)$, the numerical problem must be of the form

$$\frac{d\vec{x}}{dt} = \vec{F}(\vec{x}) \quad (1)$$

where $\vec{F}(\vec{x})$ is a vector function of the vector variable \vec{x} . Finding this function can be very difficult for a complicated circuit topology, since the circuit equations usually take the form

$$\vec{\mathbb{F}}\left(\vec{x}, \frac{d\vec{x}}{dt}\right) = 0 \quad (2)$$

Numerical simulators like PSPICE routinely use a numerical engine (a “root solver”) that converts equation 2 into equation 1, which greatly increases execution time since it must be done at each time step.

It is usually found that not all the currents and voltages are needed to describe the circuit dynamics. Thus, for a simple ac circuit like the one in figure 5: only two differential equations are needed, the currents through the two inductors. These currents are said to be the *state variables* of the circuit. In general, state variables are defined as the *smallest set of electrical quantities that can completely specify the circuit performance*.

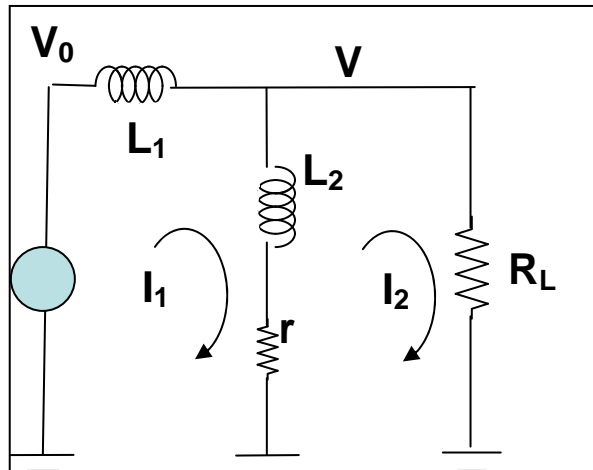


Figure 5. Two-inductor circuit.

For more complex circuits there may be multiple choices for these state variables. While currents and voltages are appropriate for resistive elements, the natural variables for capacitors and inductors are actually charges and magnetic fluxes, and these quantities are often handy alternatives to currents and voltages, especially when the circuit does not immediately admit a description using first-order differential equations.

A trivial example is a series LRC circuit (see figure 6).

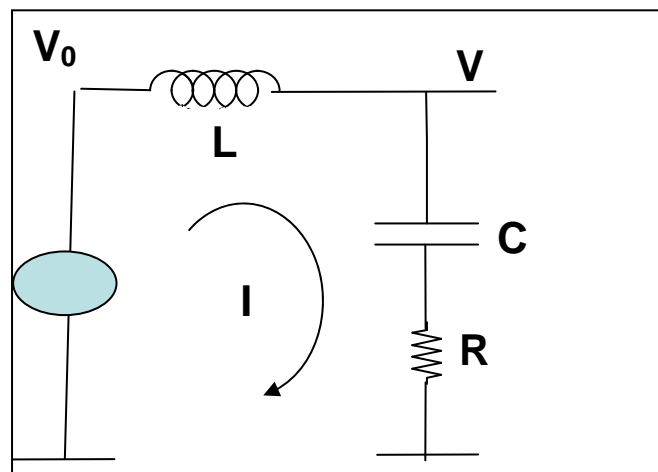


Figure 6. Series LRC circuit.

This circuit is usually treated by writing a single equation

$$V_0 = V_L + V_R + V_C \quad (3)$$

where the voltage drops are given by

$$V_L = L \frac{dI}{dt} \quad V_R = RI \quad V_C = \frac{1}{C} \int_0^t I(\tau) d\tau$$

This equation can be solved easily; however, from a numerical standpoint it has the problem that it has an integral in it, which means it is not a differential equation. Taking the derivative of equation 3 corrects this:

$$\frac{dV_0}{dt} = L \frac{d^2 I}{dt^2} + R \frac{dI}{dt} + \frac{1}{C} I$$

Although this is easily solved analytically, it is not first order and hence is problematic for numerical solution. A new choice of state variables fixes this: since the current is related to the charge on the capacitor by

$$I = \frac{dQ}{dt}$$

we can write the following system of equations:

$$\begin{aligned} \frac{dQ}{dt} &= I \\ \frac{dI}{dt} &= \frac{1}{L} V_0 - \frac{R}{L} I - \frac{1}{LC} Q \end{aligned}$$

We now have a state vector $\vec{x} = \begin{pmatrix} Q \\ I \end{pmatrix}$ to describe the circuit, and a vector function

$$\vec{F}(\vec{x}) = \begin{pmatrix} I \\ \frac{1}{L} V_0 - \frac{R}{L} I - \frac{1}{LC} Q \end{pmatrix}$$

which a simulator can accept.

It is fortunate that this choice of state variables also works for the NLTL. The appendix contains the derivation of the set of network equations for the Brown-Ikezi circuit for an NLTL with an arbitrary number of stages. This set of equations has been coded into *Mathematica*, and seems to work well – circuits with over a thousand stages have been simulated without numerical problems.

3.3 The Method of Partial Charges

In writing the network equations for this circuit, it is useful to generalize the state variables discussed above. As discussed in the appendix, a natural way to treat the NLTL circuit is by loop currents, as shown in the circuit picture at the beginning of this report. Now, the discussion in the

previous section suggests that we introduce a “charge” q_n associated with each loop current, which we define as

$$i_n = \frac{dq_n}{dt}$$

This identifies a set of state variables $\{q_1, q_2, \dots, q_N, q_L\}$ and $\{i_1, i_2, \dots, i_N, i_L\}$ for the circuit, which a differential-equation solver can handle easily. Once we have the solution to the network equations, we can get the node voltages from the obvious relation

$$V_n = V_{Cn} + r(i_n - i_{n+1})$$

where V_{Cn} is the voltage drop across the nonlinear capacitor. As discussed in Report #1, we write this voltage in the form

$$V_{Cn} = C^{-1}Q_n + \alpha Q_n^3$$

where the capacitor charge $Q_n = q_n - q_{n+1}$ mimics the behavior of the shunt current. This is a true charge, arising from the flow of current into and out of the shunt branch.

It is remarkable that when this decomposition of Q_n into “partial charges” q_n is made, preliminary simulation results reveal that the q_n are unphysical even though their difference is not. When a NLTL is pulsed by a finite voltage signal, after a long time all the variables q_n are nonzero and identical in value. This means that the currents and true charges on the capacitors must vanish, as they should in a dissipative network (i.e., one with resistors). This rather mysterious result has no impact on the modeling results, but it is an interesting consequence of the freedom to assign state variables to a nonlinear circuit.

4. Experimental Fitting of Resistive Losses in the NLTL Based on Loss Tangent Data

Accurate determination of losses in ferroelectric materials such as BST is extremely difficult, especially over a wide frequency range. Because such losses have a major impact on the performance of our NLTL, particular care was taken to identify a reasonable number for the single parameter we use to characterize these losses – the resistance r shown in the circuit (see figure 7).

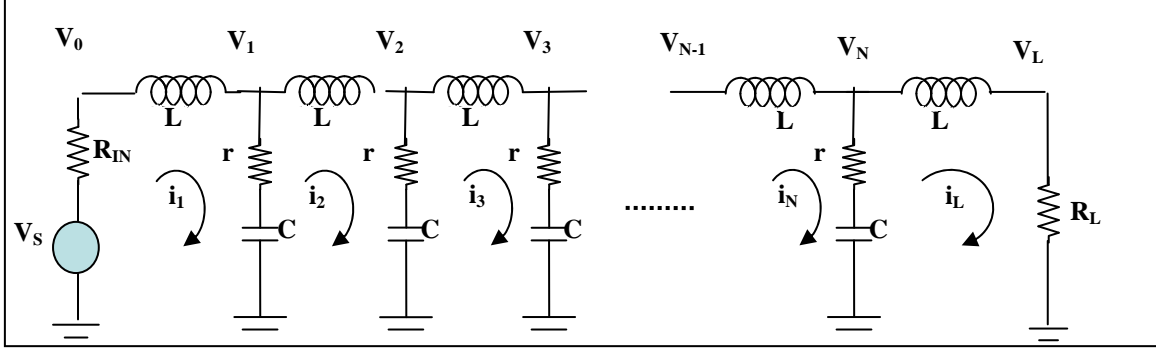


Figure 7. Placement of resistors in Brown-Ikezi NLTL circuit.

Neither Brown nor Ikezi provide any information about this number, although Brown suggests that he used loss-tangent data to obtain a value for r (note that he uses the circuit shown above, just as we do). Because loss-tangent data does not directly translate into r , a procedure was developed for connecting these numbers, which will be described. All the simulations performed will be based on numbers obtained from this procedure.

Frequency dependent measurements of BST parameters usually are based on capacitance measurements made on fabricated capacitor structures. This procedure is typified by the work of Rimai et al., (9), who used capacitors to measure dielectric constant and loss tangent as a function of frequency. They fitted their data to the following functional form:

$$\varepsilon = \varepsilon_0 \left\{ 1 + \chi_0 - \frac{j\omega\sigma - \omega^2}{\omega_t^2 + j\omega\sigma - \omega^2} [\chi_0 - \chi_\infty] \right\}$$

where the parameters ω_t , χ_0 , χ_∞ and σ are used to fit the data. The values of these parameters they found for their particular BST samples were:

$$\omega_t = 1020 \text{ GHz}$$

$$\chi_0 = 1900$$

$$\chi_\infty = 6$$

$$\sigma = 2.5\omega_t$$

Now, the loss tangent is defined in most of the ferroelectric literature as follows:

$$\tan \delta(\omega) = \frac{\text{Im} \varepsilon(\omega)}{\text{Re} \varepsilon(\omega)}$$

so its values are obtained by finding

$$\begin{aligned}
\operatorname{Re} \varepsilon(\omega) &= \varepsilon_0 \operatorname{Re} \left\{ \frac{\omega_t^2 (1 + \chi_0) + (j\omega\sigma - \omega^2)(1 + \chi_\infty)}{\omega_t^2 + j\omega\sigma - \omega^2} \right\} \\
&= \varepsilon_0 \operatorname{Re} \left\{ \frac{[\omega_t^2 (1 + \chi_0) - \omega^2 (1 + \chi_\infty) + j\omega\sigma(1 + \chi_\infty)][\omega_t^2 - \omega^2 - j\omega\sigma]}{[\omega_t^2 - \omega^2]^2 + \omega^2 \sigma^2} \right\} \\
&= \varepsilon_0 \left\{ \frac{[\omega_t^2 (1 + \chi_0) - \omega^2 (1 + \chi_\infty)][\omega_t^2 - \omega^2] + \omega^2 \sigma^2 (1 + \chi_\infty)}{[\omega_t^2 - \omega^2]^2 + \omega^2 \sigma^2} \right\}
\end{aligned}$$

and likewise

$$\begin{aligned}
\operatorname{Im} \varepsilon(\omega) &= \varepsilon_0 \operatorname{Im} \left\{ \frac{\omega_t^2 (1 + \chi_0) + (j\omega\sigma - \omega^2)(1 + \chi_\infty)}{\omega_t^2 + j\omega\sigma - \omega^2} \right\} \\
&= \varepsilon_0 \operatorname{Im} \left\{ \frac{[\omega_t^2 (1 + \chi_0) - \omega^2 (1 + \chi_\infty) + j\omega\sigma(1 + \chi_\infty)][\omega_t^2 - \omega^2 - j\omega\sigma]}{[\omega_t^2 - \omega^2]^2 + \omega^2 \sigma^2} \right\} \\
&= \varepsilon_0 \omega \sigma \left\{ \frac{(1 + \chi_\infty)\omega_t^2 - (1 + \chi_\infty)\omega^2 - \omega_t^2(1 + \chi_0) + \omega^2(1 + \chi_\infty)}{[\omega_t^2 - \omega^2]^2 + \omega^2 \sigma^2} \right\} \\
&= -\varepsilon_0 \omega \sigma \frac{\omega_t^2 (\chi_0 - \chi_\infty)}{[\omega_t^2 - \omega^2]^2 + \omega^2 \sigma^2}
\end{aligned}$$

Then the loss tangent is given by

$$\begin{aligned}
\tan \delta &= -\frac{\operatorname{Im} \varepsilon(\omega)}{\operatorname{Re} \varepsilon(\omega)} = \frac{\varepsilon_0 \omega \sigma \frac{\omega_t^2 (\chi_0 - \chi_\infty)}{[\omega_t^2 - \omega^2]^2 + \omega^2 \sigma^2}}{\varepsilon_0 \left\{ \frac{[\omega_t^2 (1 + \chi_0) - \omega^2 (1 + \chi_\infty)][\omega_t^2 - \omega^2] + \omega^2 \sigma^2 (1 + \chi_\infty)}{[\omega_t^2 - \omega^2]^2 + \omega^2 \sigma^2} \right\}} \\
&= \omega \sigma \frac{\omega_t^2 (\chi_0 - \chi_\infty)}{[\omega_t^2 (1 + \chi_0) - \omega^2 (1 + \chi_\infty)][\omega_t^2 - \omega^2] + \omega^2 \sigma^2 (1 + \chi_\infty)}
\end{aligned}$$

The expressions above are valid from dc to near-IR frequencies, but for microwave applications they are useful primarily at low frequencies. It is therefore convenient to take the following limit:

$$\omega \rightarrow 0 \Rightarrow \tan \delta \rightarrow \omega \sigma \frac{\chi_0 - \chi_\infty}{\omega_t^2 (1 + \chi_0)}$$

The problem with this expression is that, unlike a true resistance, this quantity depends linearly on frequency.

In order to make contact with our NLTL, we look at the capacitance of a BST layer with area A and thickness h and this kind of dielectric constant, and compute the corresponding impedance of the layer:

$$C = \varepsilon(\omega) \frac{A}{h} = \varepsilon_0 \left\{ \frac{\omega_t^2 (1 + \chi_0) + (j\omega\sigma - \omega^2)(1 + \chi_\infty)}{\omega_t^2 + j\omega\sigma - \omega^2} \right\} \frac{A}{h}$$

$$Z = \frac{1}{j\omega C} = \frac{1}{j\omega\varepsilon_0} \left\{ \frac{\omega_t^2 + j\omega\sigma - \omega^2}{\omega_t^2 (1 + \chi_0) + (j\omega\sigma - \omega^2)(1 + \chi_\infty)} \right\} \frac{h}{A}$$

A low-frequency expansion of Z gives:

$$Z = \frac{1}{j\omega\varepsilon_0 (1 + \chi_0)} \left\{ \frac{1 + j \frac{\omega}{\omega_t^2} \sigma - \frac{\omega^2}{\omega_t^2}}{1 + \left(j \frac{\omega}{\omega_t^2} \sigma - \frac{\omega^2}{\omega_t^2} \right) \left(\frac{1 + \chi_\infty}{1 + \chi_0} \right)} \right\} \frac{d}{A}$$

$$\approx \frac{1}{j\omega\varepsilon_0 (1 + \chi_0)} \frac{d}{A} \left\{ 1 + \left(j \frac{\omega}{\omega_t^2} \sigma - \frac{\omega^2}{\omega_t^2} \right) \left(1 - \frac{1 + \chi_\infty}{1 + \chi_0} \right) \right\}$$

$$\approx \frac{1}{j\omega\varepsilon_0 (1 + \chi_0)} \frac{d}{A} \left\{ 1 + j \frac{\omega}{\omega_t^2} \sigma \left(\frac{\chi_0 - \chi_\infty}{1 + \chi_0} \right) \right\} = \frac{1}{j\omega\varepsilon_0 (1 + \chi_0)} \frac{d}{A} + \frac{\sigma}{\varepsilon_0 \omega_t^2} \frac{\chi_0 - \chi_\infty}{(1 + \chi_0)^2} \frac{d}{A}$$

$$\equiv \frac{1}{j\omega C_0} + r$$

and thus it is clear that Z is the impedance of a capacitance C_0 and a resistance r connected in series. This justifies our circuit topology, which is gratifying, but more importantly it gives us a formula for r :

$$\begin{aligned}\tan \delta &= \omega \sigma \frac{\chi_0 - \chi_\infty}{\omega_t^2 (1 + \chi_0)} \Rightarrow \frac{\sigma}{\epsilon_0 \omega_t^2} \frac{\chi_0 - \chi_\infty}{(1 + \chi_0)^2} = \frac{1}{\omega \epsilon_0 (1 + \chi_0)} \omega \sigma \frac{\chi_0 - \chi_\infty}{\omega_t^2 (1 + \chi_0)} \\ \Rightarrow r &= \lim_{\omega \rightarrow \infty} \frac{d}{A} \frac{1}{\omega \epsilon_0 (1 + \chi_0)} \tan \delta \Rightarrow Z = \frac{1}{j \omega C_0} (1 + j \tan \delta) \\ \Rightarrow r &= \frac{\tan \delta}{\omega C_0}\end{aligned}$$

This simple result almost gets us where we want to be. However, in order for r to be constant we need the linear frequency dependence of $\tan \delta$ alluded to above. The variation of $\tan \delta$ observed in experiment is not encouraging: the following plots (see figure 8) are given in the paper by Vorobiev and Gevorgian (10):

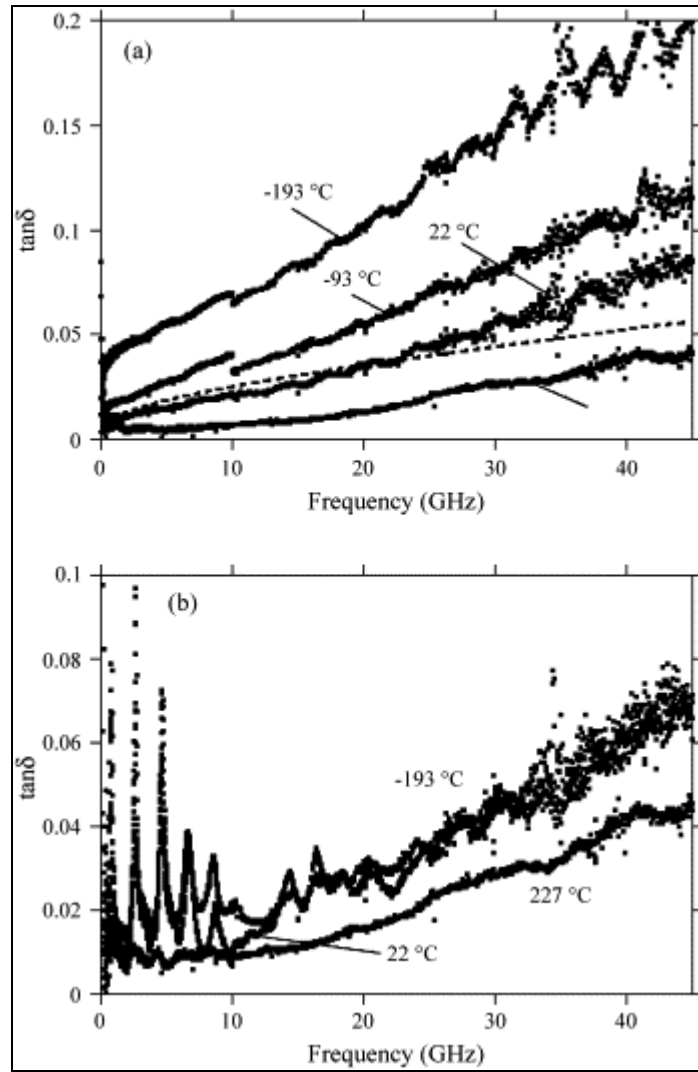


Figure 8. Loss tangent of a BST varactor vs. frequency at different temperatures without (a) and under 20 V dc bias (b). The dotted line represents the $\tan \delta \sim \omega^{1/3}$ power law.

These authors predict a peculiar dependence $\tan \delta \sim \omega^{1/3}$ for the loss tangent, which is not very useful for our applications. Since the data used to make these plots was unavailable, the crude approach of connecting the points $\omega = 0$, $\tan \delta = 0$, and $\omega = 40$ GHz, $\tan \delta = 0.07$ with a straight line was used, and its slope, along with a value of C_0 appropriate for our structure, was inserted in the formula $r = \frac{\tan \delta}{\omega C_0}$. Using the endpoint data $\tan \delta = .07$ at $f = 40$ GHz gives

$$r = \frac{h}{A} \frac{(.07)}{2\pi(4 \times 10^{10} \text{ s}^{-1})(8.85 \times 10^{-14} \text{ f cm}^{-1})(5000)}$$

$$1 \text{ f} = 1 \text{ Ohm}^{-1}\text{-s} \Rightarrow r = \frac{h}{A} \frac{(.07)}{2\pi(4 \times 10^{10} \text{ s}^{-1})(8.85 \times 10^{-14} \text{ Ohm}^{-1}\text{-s cm}^{-1})(5000)}$$

$$= \frac{h}{A} \frac{1}{\text{cm}} \frac{(.07)}{2\pi(4 \times 10^{10})(8.85 \times 10^{-14} \text{ cm}^{-1})(5000)} \text{ Ohm}$$

In all the simulations to date, Brown's numbers have been used for the line dimensions. In his notation, $A = wd = (2.5 \text{ cm})(.3 \text{ cm}) = .75 \text{ cm}^2$, $h = .55 \text{ cm}$, which gives

$$r = \frac{.55 \text{ cm}}{.75 \text{ cm}^2} \frac{(.07)}{2\pi(4 \times 10^{10})(8.85 \times 10^{-14} \text{ cm}^{-1})(5000)} \text{ Ohm}$$

$$= \frac{(.07)(.55)}{(6.2832)(.75)(4 \times 10^{10})(8.85 \times 10^{-14})(5000)} \text{ Ohm} = .00046 \text{ Ohm}$$

As better data is obtained, this approach can be refined. For now, however, the value obtained is suitable for simulations.

5. Realistic Antenna Coupling Via an RC Circuit

The code written in Mathematica mimics that of both Brown and Ikezi, i.e., it is based on a simple series-parallel circuit model for the NLTL (see figure 9).

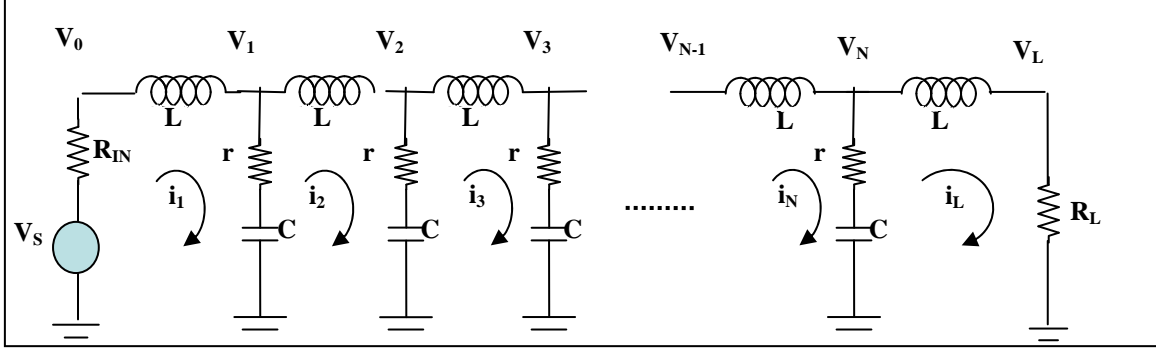


Figure 9. NLTL with simple resistive load.

For the applications under study, this transmission line is excited by transient signals, i.e., pulses. Because pulse shapes are nonperiodic functions, there is a potential for a lossless transmission line to support signals with dc levels. However, a real antenna cannot pass a dc level, so that this problem is clearly mathematical rather than physical. To represent the antenna more realistically, a series capacitance can be included in the load, so the circuit becomes (see figure 10).

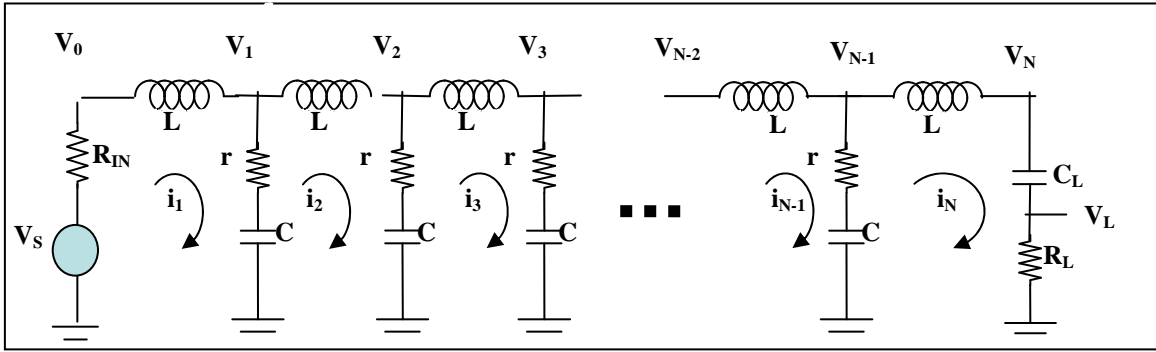


Figure 10. NLTL with RC circuit load to simulate antenna reactance.

The inductor voltage drops are related to the loop currents as stated previously. In particular, at the last stage of the transmission line we still have

$$L \frac{di_N}{dt} = V_{N-1} - V_N$$

This last stage sees a voltage divider described by the equation

$$\begin{aligned} V_N &= R_L i_N + C_L^{-1} q_N \\ \Rightarrow L \frac{di_N}{dt} &= V_{N-1} - R_L i_N - C_L^{-1} q_N \\ &= \Gamma [q_{N-1} - q_N] + r (i_{N-1} - i_N) - R_L i_N - C_L^{-1} q_N \\ &= C^{-1} q_{N-1} - (C^{-1} + C_L^{-1}) q_N + \alpha (q_{N-1} - q_N)^3 + r i_{N-1} - (r + R_L) i_N \end{aligned}$$

We can use these expressions to eliminate the voltages entirely, which gives us a set of network equations in terms of q_n and i_n alone:

$$\begin{aligned}
L \frac{di_1}{dt} &= V_S(t) - R_{in} i_1 - \Gamma[q_1 - q_2] - r(i_1 - i_2) \\
&\vdots \\
L \frac{di_{n-1}}{dt} &= \Gamma[q_{n-2} - q_{n-1}] - \Gamma[q_{n-1} - q_n] + r(i_{n-2} - 2i_{n-1} + i_n) \\
L \frac{di_n}{dt} &= \Gamma[q_{n-1} - q_n] - \Gamma[q_n - q_{n+1}] + r(i_{n-1} - 2i_n + i_{n+1}) \\
\Rightarrow L \frac{di_{n+1}}{dt} &= \Gamma[q_n - q_{n+1}] - \Gamma[q_{n+1} - q_{n+2}] + r(i_n - 2i_{n+1} + i_{n+2}) \\
&\vdots \\
L \frac{di_{N-1}}{dt} &= \Gamma[q_{N-2} - q_{N-1}] - \Gamma[q_{N-1} - q_N] + r(i_{N-2} - 2i_{N-1} + i_N) \\
L \frac{di_N}{dt} &= C^{-1} q_{N-1} - (C^{-1} + C_L^{-1}) q_N + \alpha(q_{N-1} - q_N)^3 + r i_{N-1} - (r + R_L) i_N
\end{aligned}$$

Then the set of network equations is completed by

$$\begin{aligned}
i_n &= \frac{dq_n}{dt} \\
i_N &= \frac{dq_N}{dt}
\end{aligned}$$

and

$$V_L = R_L i_N$$

It is no longer convenient to nondimensionalize these equations because there are two different capacitors in the system.

6. Description of Mathematica Code

The circuit equations are easily converted to Mathematica™ form, which has a universal numerical differential equation solver called NDSolve. The only challenging problem about setting up these equations is to generate the code for an arbitrary number of layers. This can be done piecemeal by separating the equations into starting, intermediate, and ending segments. Each of these segments involves a set of equations, as shown above:

$$\begin{array}{l}
\text{Starting segment:} \\
\text{Intermediate segment:} \\
\text{Ending segment:}
\end{array}
\left\{
\begin{array}{l}
L \frac{di_1}{dt} = V_S(t) - R_{in} i_1 - \Gamma[q_1 - q_2] - r(i_1 - i_2) \\
\frac{dq_1}{dt} = i_1 \\
\vdots \\
L \frac{di_{n-1}}{dt} = \Gamma[q_{n-2} - q_{n-1}] - \Gamma[q_{n-1} - q_n] + r(i_{n-2} - 2i_{n-1} + i_n) \\
\frac{dq_{n-1}}{dt} = i_{n-1} \\
L \frac{di_n}{dt} = \Gamma[q_{n-1} - q_n] - \Gamma[q_n - q_{n+1}] + r(i_{n-1} - 2i_n + i_{n+1}) \\
\frac{dq_n}{dt} = i_n \\
L \frac{di_{n+1}}{dt} = \Gamma[q_n - q_{n+1}] - \Gamma[q_{n+1} - q_{n+2}] + r(i_n - 2i_{n+1} + i_{n+2}) \\
\frac{dq_{n+1}}{dt} = i_{n+1} \\
\vdots \\
L \frac{di_N}{dt} = C^{-1} q_{N-1} - (C^{-1} + C_L^{-1}) q_N + \alpha (q_{N-1} - q_N)^3 + r i_{N-1} - (r + R_L) i_N \\
\frac{dq_N}{dt} = i_N
\end{array}
\right.$$

The resulting code looks as follows:

```

eqs=Table[{ cd[i]' [tau] (1+LM (s[i-1] [tau]^2+s[i] [tau]^2+s[i+1] [tau]^2-s[i-1] [tau] s[i] [tau] - s[i] [tau] s[i+1] [tau] -s[i-1] [tau] s[i+1] [tau])) (s[i-1] [tau] - 2s[i] [tau]+s[i+1] [tau]) +Qc (cd[i-1] [tau] - 2cd[i] [tau]+cd[i+1] [tau]), s[i]' [tau] cd[i] [tau] }, {i, 2, NN-1}];
eqst={cd[1]' [tau] U0 [tau] - (s[1] [tau] -s[2] [tau]) -LM (s[1] [tau] - s[2] [tau])^3-Qc (cd[1] [tau] -cd[2] [tau]), s[1]' [tau] cd[1] [tau]};
eqfn={cd[NN]' [tau] (s[NN-1] [tau] -s[NN] [tau]) +LM (s[NN-1] [tau] - s[NN] [tau])^3-gamma s[NN] [tau] +Qc cd[NN-1] [tau] - (Qc+QL) cd[NN] [tau], s[NN]' [tau] cd[NN] [tau]};
eqp=Prepend[eqs, eqst];
equ=Flatten[Append[eqp, eqfn]];
init=Flatten[Table[{s[i] [0] 0, cd[i] [0] 0}, {i, 1, NN}]];
NDSL=Flatten[Prepend[init, equ]];
vlist=Flatten[Table[{s[i], cd[i]}, {i, NN}]];
sol=NDSolve[NDSL, vlist, {tau, 0, 500}, MaxSteps->Infinity];

```

In this code, the function Table generates an arbitrary number of intermediate equations, which describe the interior of the transmission line. This set of equations (the intermediate segment) is concatenated with the starting and ending segments, and the full set is solved by the numerical routine. The result is a list of currents and charges for the circuit elements, which can be examined and plotted.

The translation of this mathematical routine into a MatLab™ code will be straightforward, provided that MatLab™ has utilities which can generate equation lists for arbitrary numbers of layers. Implementing this transfer will be an important deliverable when work on this project resumes.

7. Results of Preliminary Simulations

To date, the numerical code has been exercised in ways that bring out the physics of the frequency translation rather than parameter extraction; this focus lends credence to the correctness of the code results, which can be nonintuitive. Indeed, much of the value of numerical work lies in creating intuition where none existed before.

Simulations were performed using a series of pulses based on Ikezi's normalized trapezoidal pulse shape. I chose this pulse shape because it incorporates simply three numbers that characterize any pulse: a rise time, a pulse "width", and a fall time. Thus, consider a pulse of almost triangular shape (see figure 11).

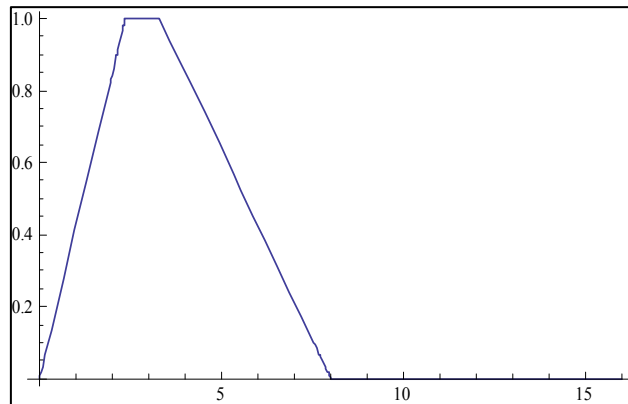


Figure 11. Ikezi normalized short test pulse shape; time scale in NLTL low-frequency single-stage periods.

For a lossless NLTL, the time scale is measured by the period of the LC stages. In units of this period, the rise time of this pulse is 2 periods, its duration 1 period, and its fall time 5 periods. Let us choose L and C such that the period was 13 ns, and pulse the line with a 50 V signal, whose total pulse length is 104 ns. This low voltage should cause the line to respond like a linear filter. Plotting the time dependence of the voltage at the antenna end of the line gives (see figure 12).

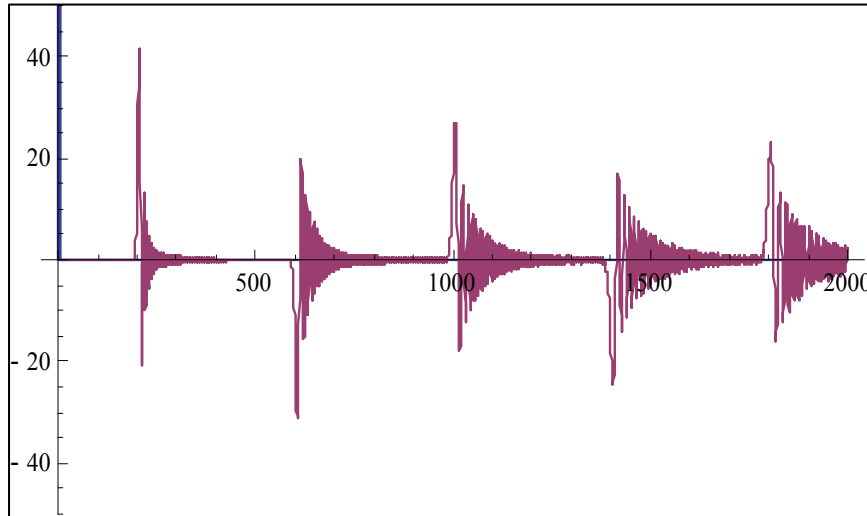


Figure 12. Low voltage response to figure 11 test pulse at end of NLTL.

The oscillatory tails following the pulse front exhibit typical dispersive behavior of the line. When the pulse voltage is increased to 6 kV, the following plot results (see figure 13), which reveals the evolution of solitons.

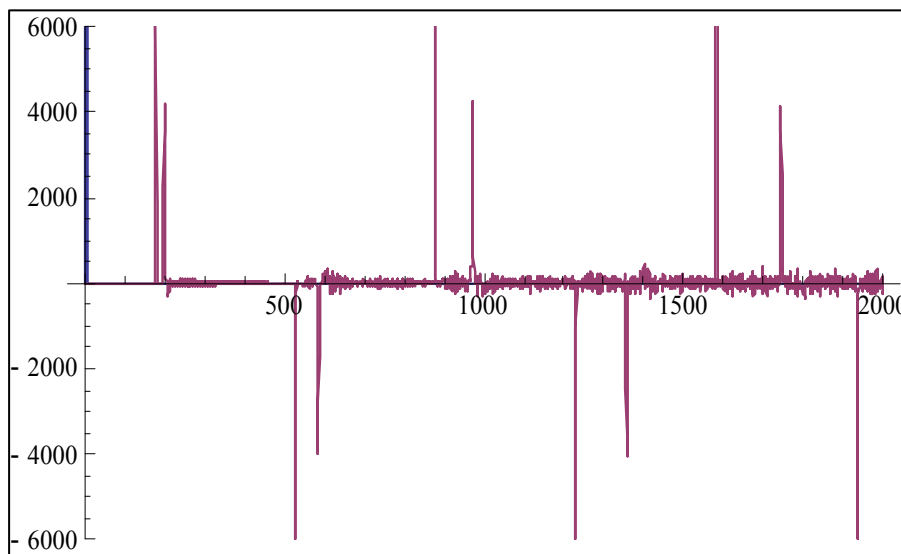


Figure 13. High voltage response to figure 11 test pulse at end of NLTL; note solitons.

Increasing the 50 V pulse width to 10 periods (see figure 14).

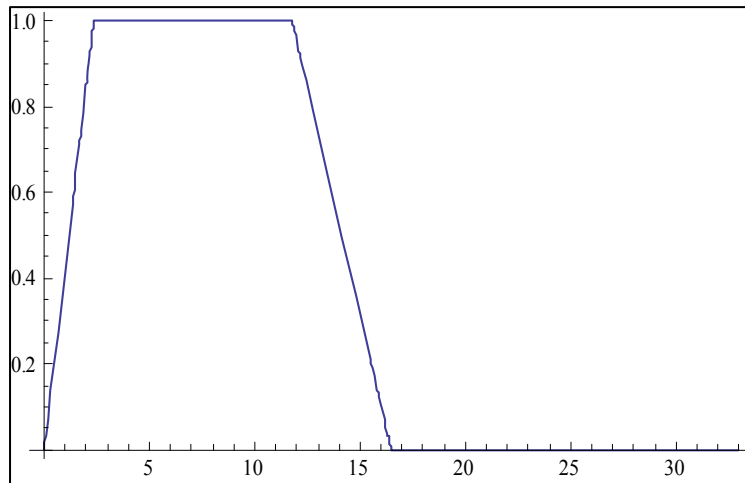


Figure 14. Ikezi normalized long test pulse shape.

Gives a linear response of the form (see figure 15).

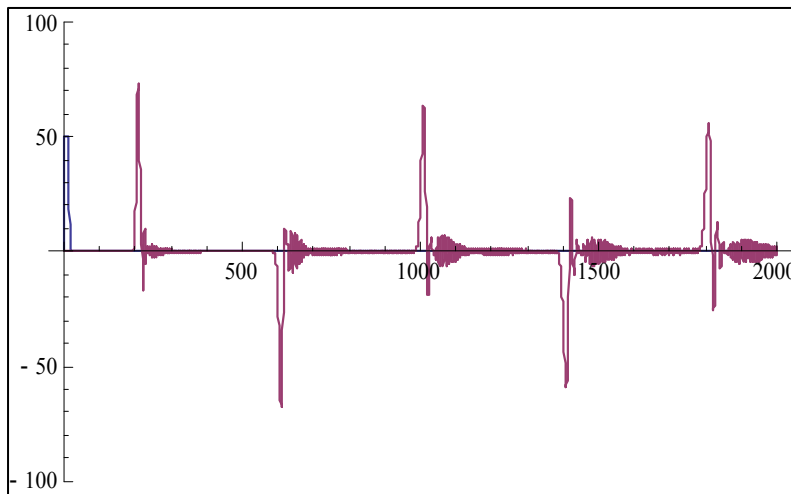


Figure 15. Low voltage response to figure 14 test pulse at end of NLTL.

The longer duration has separated the rise-time regions, producing spikes; these are not solitons, however, since the voltage is too low. Increasing the voltage to 5 kV shows multiple soliton generation. This suggests that long-duration pulses are better than short-duration ones for producing multiple solitons (see figure 16).

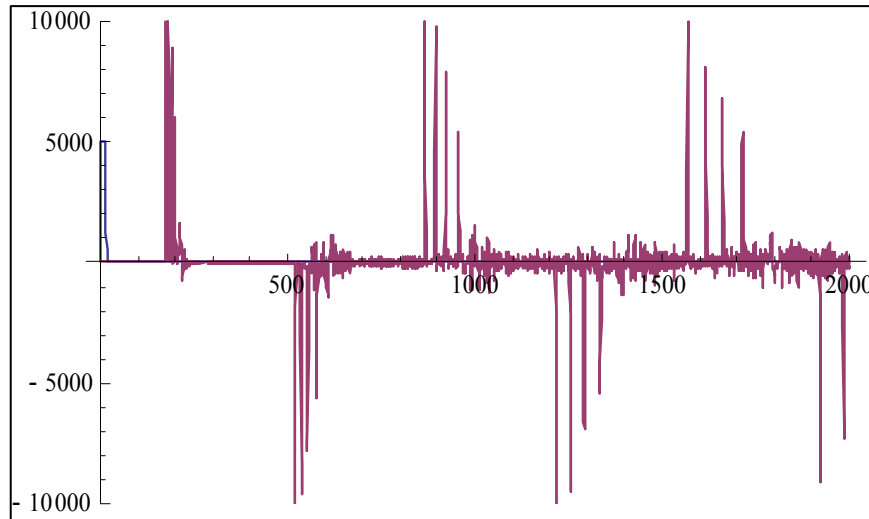


Figure 16. High voltage response to figure 14 test pulse at end of NLTL; note solitons.

8. Movies of NLTL Interior

There are a number of features of these plots that require explanation. To this end, I have used a very handy feature of the Mathematica™ code to examine the interior of the NLTL as a pulse propagates within it. Because they exhibit only the output voltage, these plots treat the device as a “black box”, whose mysterious generation of alternating “bursts” of pulses is hard to understand. However, because the code simultaneously evaluates voltages and currents at every node, i.e., at every layer of the structure, these nodal quantities can be exhibited as “maps” of the voltage/current profile at each time step, which can be displayed as “movies” of the line interior.

Multiple movies were made to examine the overall propagation of signals in the line. Two of these movies are included in this report, on a companion CDs for the hard copies; the data files they are based on are very large (~.5 Gb). Being able to examine the interior immediately reveals the origin of the bursts: the initial drive pulse propagates to the end of the line with a certain average velocity, disintegrating as it propagates. Once it reaches the end of the line, it is reflected. In the simulations I have made to date the antenna impedance is high, which makes the end of the line look like an open circuit. This causes the reflected signal to add to the incident signal, doubling the total amplitude. The first pulse burst marks the arrival of the distorted pulse at the end. The pulse then returns to the source, where the voltage is fixed, which makes the source look like a short circuit; this causes the reflected voltage to become negative. The negative reflected pulse then returns to the far end of the line, producing the negative-going second burst, which is once again doubled in magnitude. This cycle repeats until the pulse has given up all its energy to the load, in small increments because the load impedance is high.

The first movie is of a long (120 ns) low-voltage (50 V) pulse, which changes shape as it propagates due purely to dispersion. Because the propagation velocity of a sinusoidal signal in a dispersive medium depends on frequency, the high-frequency components, which contribute to the rapid rise and fall times of the pulse, “dephase” during the propagation and produce the oscillations shown. Note that the frequency spectrum tends to redistribute energy to lower frequencies and not higher ones. The second movie is of a pulse with the same duration but much higher voltage (5 kV). The high-voltage pulse disintegrates into what appear to be solitons before reaching the end of the line. However, their shape is not stable – there is an unexpected oscillation in the soliton height. Compare these pulses with the superficially similar “ripples” in the low-voltage pulse, which are more or less stationary in shape. The origin of the high-voltage shape instability is unclear; while it is tempting to identify it with the “modulation instability” of soliton trains discussed in the literature, it could also be related to the discrete, i.e., “circuit”, nature of the model. Although this effect is small, and hence of no engineering importance, it is scientifically interesting, and cautionary given the tendency for any kind of pulse compression or amplification to be referred in the literature to as “soliton generation”.

9. Systems Issues

Although this modeling effort was preliminary, it is useful to bound the behavior of the NLTL based on optimal predictions of its performance. These predictions can only be based on the information available now, but they serve as a guide for future efforts.

1. Maximum output power. Clearly we can use the breakdown field of the ferroelectric to estimate this quantity. In BST ceramics this field can approach 750 kV/cm. Assume that the line is a BST/alumina-filled parallel-plate waveguide, which propagates a TEM wave with electric and magnetic fields \vec{E} and \vec{H} perpendicular and parallel to the conducting walls of the guide (top and bottom), respectively. At high power levels the dielectric constant of the BST saturates, dropping from 5500 for a very good sample to about 120. Then for a uniform line made of lossless material the characteristic impedance at large signal levels is $Z_C = 377 / \sqrt{\epsilon} = 377 / \sqrt{120} = 34.4$ ohms. Since the power flux is given by the Poynting vector, the power flux at breakdown is

$$\begin{aligned} \wp &= \hat{n} \cdot \vec{E} \times \vec{H} = EH = Z^{-1} E^2 = (34.4 \Omega)^{-1} (7.5 \times 10^5 \text{ V/cm})^2 \\ &= 16.3 \text{ GW/cm}^2 \end{aligned}$$

Since the lines we fabricated had cross-sections of $2.5 \times .3 = .75 \text{ cm}^2$, one of our lines could handle ~ 12 GW. Note, however, that the inevitable impedance mismatch with the antenna due to the nonlinearity will reduce this, probably by about 50%, so ~ 6 GW is a more realistic number.

2. Maximum frequency: this is hard to specify without referring to geometric, i.e., manufacturing issues. The modeling we did was based on a formula Ikezi quotes in one of his General Atomics papers (Ikezi et al., Appl. Phys. Lett. **58**, 986 (1991)), derived from simulation data. The structure he starts with is a parallel-plate waveguide with BST sheets in it, i.e., the one described above. His initial design numbers involve the linear modes of this structure, which is in essence a band-stop filter. As such, it allows frequencies to propagate that are below a certain maximum frequency – he calls it ω_b – and blocks signals with higher frequencies within a “stop band”. His nonlinear simulations reveal that this maximum frequency also determines the oscillation frequency ω_{osc} from the empirical formula

$$\frac{\omega_{osc}}{\omega_b} = 1.25 + 1.5 \log_{10} \left(\frac{E}{E_0} \right)$$

where the field E is the maximum field in the line, and E_0 is a material-dependent constant with the dimensions of field; for BST this number is around 10 kV/cm. This frequency ω_b depends mostly on the widths of the ferroelectric and dielectric slabs, and their linear dielectric constants. If we assume the ferroelectric is BST6-4, i.e., with 60% barium and 40% strontium, ϵ for his material is 5500 at room temperature, i.e., 20 °C (this is an optimistic number); at lower temperatures it is higher (the Curie temperature is 0 °C), but clearly room temperature is appropriate for our application. Given the volume constraints imposed by the latter, the optimal transmission line length is probably about 15 cm. To increase ω_b , we want to make the layers as thin as possible. However, we found that layers thinner than .1 mm are too fragile to handle, so let us assume the ferroelectric layers are .1 mm thick. If we have 15 cm to fit the transmission line into the weapon, and we want 100 layers of each kind of material, this implies a total thickness of ferroelectric of 1 cm, leaving 14 cm for dielectric, or 1.4 mm per layer. Then using the formula above along with Ikezi’s linear-design formula (equation 3 of the Applied Physics paper mentioned above), we find the resulting bandstop filter corresponds to an ω_{osc} of 3.4 GHz.

3. Pulse repetition frequency. This can be estimated based on the observation that in this type of line, impedance mismatch with the antenna is inevitable due to the nonlinearity. This in turn gives rise to reflections, which return to the source and interfere with subsequent pulses. The safe thing to do is to wait until all these have died away. If we define “died away” to mean that only 1% of the original power is left after N reflections, and the reflected power is 50% = .5 of the incident power for each reflection, we are saying that $(.5)^N = .01$, or $N =$ between 6 and 7. Now, the maximum propagation velocity of a pulse in the transmission line is the velocity of light for the reduced (saturated) high-field dielectric constant, which is 120 for BST at high fields. This velocity is 2.7×10^9 cm/s, so that for a 15 cm line we need 7 round trips or a distance of 210 cm, which takes 7.7×10^{-8} s = 77 ns. Then the PRF is the reciprocal of this, or 13 MHz.

Now, suppose we have a train of 30 pulses coming at a rate of 3.4 GHz. Then the time between pulses is .29 ns and hence, the total duration of the pulse train is $30 \times .29 = 8.8$ ns. This implies a duty cycle of 11%. Then the time it takes for the first pulse to hit the antenna is 5.6 ns, and the time to return to the source is 11.1 ns. Since this is greater than 8.8 ns, all the pulses in the train will be transmitted to the antenna before the first reflected pulse returns to the source. Since the power is 6 GW, over a period of 8.8 ns the pulse train delivers 53 J to be radiated by the antenna. If the pulser can supply a kilojoule of energy, 19 of these pulse trains can be generated for a total dwell time of 1.46 μ s.

Summary:

Max power:	6 GW
Max frequency	3.4 GHz
PRF	13 MHz
Time between pulses	290 ps
No. of cycles of 3.4 GHz/train	30
Duration of pulse train	8.8 ns
Energy/pulse	53 J
No. of pulse trains in dwell	19
Dwell time	1.46 μ s

10. Conclusions

The results of this work validate the previous work of Ikezi and, to a lesser extent, Brown, and show that we now have a useful numerical tool for studying NLTL and guiding efforts to fabricate them. Future work will center on parameter studies for designing and optimizing the performance of these devices as HPM sources.

11. References

1. Gonzalez, G., *Microwave Transistor Amplifiers*; Prentice Hall Inc.: Englewood Cliffs, NJ, 1984.
2. Qiu, J. X.; Judy, D.; Pulskamp, J. S.; Polcawich, R. G.; Kaul, R.; Crowne, F., Characterization of Nonlinear Behavior in a Tunable Phase Shifter Using Ferroelectric PZT Thin-Film Capacitors and Its Effect on System Performance. *Microwave Symposium Digest, 2009, MTT '09. IEEE MTT-S International 7-12 June 2009*, 341.
3. Landauer, R. *IBM Journal* **1960**, *4*, 391.
- 3a. An early description of such a transmission line can be found in R. V. Khokhlov, *Radiotekhnika i Elektronika* **1961**, *6*, 917.
- 3b. Champlin, K. S.; Singh, D. R. *IEEE Trans. Microwave Theory and Techniques* **1986**, *MTT-34*, 351; Rodwell, M.J.W.; Bloom, S. M.; Auld, B. A. *Electronics Letters* **1987**, *23*, 110; Rodwell, M.J.W.; Madden, C. J.; Khuri-Yakub, B. T.; Bloom, D. M.; Pao, Y. C.; Gabriel, N. S.; Swierkowski, S. P. *Electronics Letters* **1988**, *24*, 101; Madden, C. J.; Rodwell, M.J.W.; Marsland, R. A.; Bloom, D. M. *IEEE Electron Device Letters* **1988**, *9*, 303; Yu, R. Y.; Case, M.; Kamegawa, M.; Sundaram, M.; Rodwell, M.J.W.; Gossard, A. W. *Electronics Letters* **1990**, *26*, 951; Marsland, R. A.; Sharouri, M. S.; Bloom, D. M. *Electronics Letters* **1990**, *26*, 1237; Carman, E.; Giboney, K.; Case, M.; Kamegawa, M.; Yu, Ruai; Abe, K.; Rodwell, M.J.W.; Franklin, J. *IEEE Microwave and Guided Wave Letters* **1991**, *1*, 28.
4. Ikezi, H. J. *Appl. Phys.* **1988**, *64*, 3273; Ikezi, H.; Wojtowicz, S. S.; Waltz, R. E.; DeGrassie, J. S.; Baker, D. R. *J. Appl. Phys.* **1988**, *64*, 3277; Ikezi, H.; Lin-Liu, Y. R.; Ohkawa, T.; DeGrassie, J. S. *J. Appl. Phys.* **1988**, *64*, 4717; Ikezi, H.; Wojtowicz, S. S.; Waltz, R. E.; Baker, D. R. *J. Appl. Phys.* **1988**, *64*, 6836.
5. DeGrassie, J. Soliton Microwave Generator Final Technical report. prepared for the U. S. Department of Energy under Contract DE-AC03-87SF17119, New and Innovative Concepts Program in Support of the Strategic Defense Initiative, Sept. 1987 – Nov. 1989.
6. Ikezi, H.; DeGrassie, J. S.; Drake, J. *Appl. Phys. Lett.* **1991**, *58*, 986.
7. Brown, M. High Voltage Soliton Production in Nonlinear Transmission Lines and Other Pulsed Power Applications. Thesis, Oriel College, Oxford Univ., England, Sept. 1997.
8. Devonshire, A. F. *Adv. Phys.* **1954**, *3*, 85.
9. Rimai, L.; Parsons, J. L.; Hickmott, J. T.; Nakamura, T. *Phys. Rev.* **1968**, *168*, 623.

10. Vorobiev, A.; Gevorgian, S. Microwave Performance of Thin Film Ferroelectric Varactors in the Wide Temperature Range of $-223\text{ }^{\circ}\text{C}$ to $+227\text{ }^{\circ}\text{C}$. *Journal of the European Ceramic Society* **2007**, *27* (13–15), 3847–3850.

Appendix. Brown-Ikezi Network Equations

The circuit is defined using Kirchoff's law in the usual way, based on loop currents. Source and load resistances are introduced to simulate coupling to the PFN and antenna (see figure A-1).

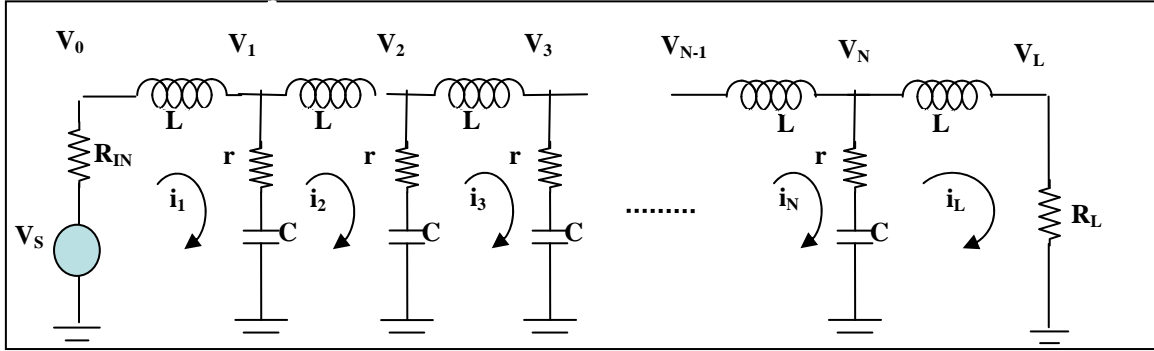


Figure A-1. Brown-Ikezi NLTL circuit.

The inductor voltage drops are related to the loop currents as follows:

$$\begin{aligned}
 L \frac{di_1}{dt} &= V_S(t) - R_{in}i_1 - V_1 \\
 &\vdots \\
 L \frac{di_{n-1}}{dt} &= V_{n-2} - V_{n-1} \\
 L \frac{di_n}{dt} &= V_{n-1} - V_n \\
 L \frac{di_{n+1}}{dt} &= V_n - V_{n+1} \\
 &\vdots \\
 L \frac{di_L}{dt} &= V_N - V_L
 \end{aligned}$$

For the shunt branches we introduce the nonlinear function $\Gamma[Q] = C^{-1}Q + \alpha Q^3$, where C is the linear term in the capacitance and α measures the circuit nonlinearity. As discussed in the text, we introduce “partial charges” q_n related to the physical currents by $i_n = \frac{dq_n}{dt}$. This gives the following expressions for the node voltages:

$$\begin{aligned}
V_0 &= V_S(t) - R_{in}i_1 \\
V_1 &= \Gamma[q_1 - q_2] + r(i_1 - i_2) \\
&\quad \vdots \\
V_{n-1} &= \Gamma[q_{n-1} - q_n] + r(i_{n-1} - i_n) \\
V_n &= \Gamma[q_n - q_{n+1}] + r(i_n - i_{n+1}) \\
V_{n+1} &= \Gamma[q_{n+1} - q_{n+2}] + r(i_{n+1} - i_{n+2}) \\
&\quad \vdots \\
V_N &= \Gamma[q_N - q_L] + r(i_N - i_L) \\
V_L &= R_L i_L
\end{aligned}$$

We can use these expressions to eliminate the voltages entirely, which gives us a set of network equations in terms of q_n and i_n alone:

$$\begin{aligned}
L \frac{di_1}{dt} &= V_S(t) - R_{in}i_1 - \Gamma[q_1 - q_2] - r(i_1 - i_2) \\
&\quad \vdots \\
L \frac{di_{n-1}}{dt} &= \Gamma[q_{n-2} - q_{n-1}] - \Gamma[q_{n-1} - q_n] + r(i_{n-2} - 2i_{n-1} + i_n) \\
L \frac{di_n}{dt} &= \Gamma[q_{n-1} - q_n] - \Gamma[q_n - q_{n+1}] + r(i_{n-1} - 2i_n + i_{n+1}) \\
\Rightarrow L \frac{di_{n+1}}{dt} &= \Gamma[q_n - q_{n+1}] - \Gamma[q_{n+1} - q_L] + r(i_n - 2i_{n+1} + i_{n+2}) \\
&\quad \vdots \\
L \frac{di_N}{dt} &= \Gamma[q_{N-1} - q_N] - \Gamma[q_N - q_L] + r(i_{N-1} - 2i_N + i_L) \\
L \frac{di_L}{dt} &= \Gamma[q_N - q_L] + r i_N - (R_L + r) i_L
\end{aligned}$$

It is useful to further reduce the terms involving the function $\Gamma[Q]$ as follows:

$$\begin{aligned}
&\Gamma[q_{n-1} - q_n] - \Gamma[q_n - q_{n+1}] = C^{-1}\{q_{n-1} - q_n\} + \alpha\{q_{n-1} - q_n\}^3 - C^{-1}\{q_n - q_{n+1}\} - \alpha\{q_n - q_{n+1}\}^3 \\
&= C^{-1}(q_{n-1} - 2q_n + q_{n+1}) + \alpha[\{q_{n-1} - q_n\}^3 - \alpha\{q_n - q_{n+1}\}^3] \\
&= [C^{-1} + \alpha(\{q_{n-1} - q_n\}^2 + \{q_{n-1} - q_n\}\{q_n - q_{n+1}\} + \{q_n - q_{n+1}\}^2)] \cdot (q_{n-1} - 2q_n + q_{n+1}) \\
&= [C^{-1} + \alpha\{q_{n-1}^2 + q_n^2 + q_{n+1}^2 - q_{n-1}q_n - q_nq_{n+1} - q_{n+1}q_{n-1}\}] \cdot (q_{n-1} - 2q_n + q_{n+1})
\end{aligned}$$

which we rewrite as follows:

$$\begin{aligned}\Pi[q_{n-1}, q_n, q_{n+1}] &= 1 + \alpha C (q_{n-1}^2 + q_n^2 + q_{n+1}^2 - q_{n-1}q_n - q_nq_{n+1} - q_{n+1}q_{n-1}) \\ \Pi_0[q_{n-1}, q_n] &= 1 + \alpha C (q_{n-1} - q_n)^2 \\ \Rightarrow \Gamma[q_{n-1} - q_n] - \Gamma[q_n - q_{n+1}] &= C^{-1} \Pi[q_{n-1}, q_n, q_{n+1}] \cdot (q_{n-1} - 2q_n + q_{n+1})\end{aligned}$$

Then the final set of network equations is

$$i_n = \frac{dq_n}{dt}$$

and

$$\begin{aligned}L \frac{di_1}{dt} &= V_S(t) - R_{in} i_1 - C^{-1} \Pi_0[q_1, q_2] \cdot (q_1 - q_2) - r(i_1 - i_2) \\ &\quad \vdots \\ L \frac{di_{n-1}}{dt} &= C^{-1} \Pi[q_{n-2}, q_{n-1}, q_n] \cdot (q_{n-2} - 2q_{n-1} + q_n) + r(i_{n-2} - 2i_{n-1} + i_n) \\ L \frac{di_n}{dt} &= C^{-1} \Pi[q_{n-1}, q_n, q_{n+1}] \cdot (q_{n-1} - 2q_n + q_{n+1}) + r(i_{n-1} - 2i_n + i_{n+1}) \\ L \frac{di_{n+1}}{dt} &= C^{-1} \Pi[q_n, q_{n+1}, q_{n+2}] \cdot (q_n - 2q_{n+1} + q_{n+2}) + r(i_n - 2i_{n+1} + i_{n+2}) \\ &\quad \vdots \\ L \frac{di_N}{dt} &= C^{-1} \Pi[q_{N-1}, q_N, q_L] \cdot (q_{N-1} - 2q_N + q_L) + r(i_{N-1} - 2i_N + i_L) \\ L \frac{di_L}{dt} &= \Pi_0[q_N, q_L] \cdot (q_N - q_L) + r i_N - (R_L + r) i_L\end{aligned}$$

where the state variables are $\{q_1, q_2, \dots, q_N, q_L\}$ and $\{i_1, i_2, \dots, i_N, i_L\}$

Dimensionless form: let $\omega_0^2 = \frac{1}{LC}$, $\tau_C = rC$, $\tau_{in} = R_{in}C$, and $\tau_L = R_L C$. Then

$$\begin{aligned}
\omega_0^{-2} \frac{di_1}{dt} &= CV_S(t) + R_{in}C i_1 - \Pi_0[q_1, q_2] \cdot (q_1 - q_2) - \tau_C (i_1 - i_2) \\
&\quad \vdots \\
\omega_0^{-2} \frac{di_{n-1}}{dt} &= \Pi[q_{n-2}, q_{n-1}, q_n] \cdot (q_{n-2} - 2q_{n-1} + q_n) + \tau_C (i_{n-2} - 2i_{n-1} + i_n) \\
\omega_0^{-2} \frac{di_n}{dt} &= \Pi[q_{n-1}, q_n, q_{n+1}] \cdot (q_{n-1} - 2q_n + q_{n+1}) + \tau_C (i_{n-1} - 2i_n + i_{n+1}) \\
\omega_0^{-2} \frac{di_{n+1}}{dt} &= \Pi[q_n, q_{n+1}, q_{n+2}] \cdot (q_n - 2q_{n+1} + q_{n+2}) + \tau_C (i_n - 2i_{n+1} + i_{n+2}) \\
&\quad \vdots \\
\omega_0^{-2} \frac{di_N}{dt} &= \Pi[q_{N-1}, q_N, q_L] \cdot (q_{N-1} - 2q_N + q_L) + \tau_C (i_{N-1} - 2i_N + i_L) \\
\omega_0^{-2} \frac{di_L}{dt} &= \Pi_0[q_N, q_L] \cdot (q_N - q_L) + \tau_C i_N - (\tau_L + \tau_C) i_L
\end{aligned}$$

Setting $\tau = \omega_0 t$, $\omega_0 \tau_C = \omega_0 rC = Q_C$, $\omega_0 \tau_{in} = \omega_0 R_{in}C = Q_{in}$, $\omega_0 \tau_L = \omega_0 R_L C = Q_L$ gives

$$\begin{aligned}
\frac{di_1}{d\tau} &= \omega_0 CV_S(\tau) - \Pi_0[q_1, q_2] \cdot \omega_0 (q_1 - q_2) - (Q_{in} + Q_C) i_1 + Q_C i_2 \\
&\quad \vdots \\
\frac{di_{n-1}}{d\tau} &= \Pi[q_{n-2}, q_{n-1}, q_n] \cdot \omega_0 (q_{n-2} - 2q_{n-1} + q_n) + Q_C (i_{n-2} - 2i_{n-1} + i_n) \\
\frac{di_n}{d\tau} &= \Pi[q_{n-1}, q_n, q_{n+1}] \cdot \omega_0 (q_{n-1} - 2q_n + q_{n+1}) + Q_C (i_{n-1} - 2i_n + i_{n+1}) \\
\frac{di_{n+1}}{d\tau} &= \Pi[q_n, q_{n+1}, q_{n+2}] \cdot \omega_0 (q_n - 2q_{n+1} + q_{n+2}) + Q_C (i_n - 2i_{n+1} + i_{n+2}) \\
&\quad \vdots \\
\frac{di_N}{d\tau} &= \Pi[q_{N-1}, q_N, q_L] \cdot \omega_0 (q_{N-1} - 2q_N + q_L) + Q_C (i_{N-1} - 2i_N + i_L) \\
\frac{di_L}{d\tau} &= \Pi_0[q_N, q_L] \cdot \omega_0 (q_N - q_L) + Q_C i_N - (Q_L + Q_C) i_L
\end{aligned}$$

Finally, setting $V_S(t) = V_m v(\tau)$, $q_n(t) = CV_m \zeta_n(\tau)$, $i_n(t) = \omega_0 CV_m \eta_n(\tau)$ gives

$$\begin{aligned}
\omega_0 CV_m \frac{d\eta_1}{d\tau} &= \omega_0 CV_m \upsilon(t) - \Pi_0[\varsigma_1, \varsigma_2] \cdot \omega_0 CV_m (\varsigma_1 - \varsigma_2) + Q_{in} \omega_0 CV_m \eta_2 - (Q_{in} + Q_C) \omega_0 CV_m \eta_1 \\
&\quad \vdots \\
\omega_0 CV_m \frac{d\eta_{n-1}}{d\tau} &= \Pi[\varsigma_{n-2}, \varsigma_{n-1}, \varsigma_n] \cdot \omega_0 CV_m (\varsigma_{n-2} - 2\varsigma_{n-1} + \varsigma_n) + Q_C \omega_0 CV_m (\eta_{n-2} - 2\eta_{n-1} + \eta_n) \\
\omega_0 CV_m \frac{d\eta_n}{d\tau} &= \Pi[\varsigma_{n-1}, \varsigma_n, \varsigma_{n+1}] \cdot \omega_0 CV_m (\varsigma_{n-1} - 2\varsigma_n + \varsigma_{n+1}) + Q_C \omega_0 CV_m (\eta_{n-1} - 2\eta_n + \eta_{n+1}) \\
\omega_0 CV_m \frac{d\eta_{n+1}}{d\tau} &= \Pi[\varsigma_n, \varsigma_{n+1}, \varsigma_{n+2}] \cdot \omega_0 CV_m (\varsigma_n - 2\varsigma_{n+1} + \varsigma_{n+2}) + Q_C \omega_0 CV_m (\eta_n - 2\eta_{n+1} + \eta_{n+2}) \\
&\quad \vdots \\
\omega_0 CV_m \frac{d\eta_N}{d\tau} &= \Pi[\varsigma_{N-1}, \varsigma_N, \varsigma_L] \cdot \omega_0 CV_m (\varsigma_{N-1} - 2\varsigma_N + \varsigma_L) + Q_C \omega_0 CV_m (\eta_{N-1} - 2\eta_N + \eta_L) \\
\omega_0 CV_m \frac{d\eta_L}{d\tau} &= \Pi_0[\varsigma_N, \varsigma_L] \cdot \omega_0 CV_m (\varsigma_N - \varsigma_L) + Q_C \omega_0 CV_m \eta_N - (Q_L + Q_C) \omega_0 CV_m \eta_L
\end{aligned}$$

or

$$\begin{aligned}
\frac{d\eta_1}{d\tau} &= \upsilon(\tau) - \Pi_0[\varsigma_1, \varsigma_2] \cdot (\varsigma_1 - \varsigma_2) + Q_{in} \eta_2 - (Q_{in} + Q_C) \eta_1 \\
&\quad \vdots \\
\frac{d\eta_{n-1}}{d\tau} &= \Pi[\varsigma_{n-2}, \varsigma_{n-1}, \varsigma_n] \cdot (\varsigma_{n-2} - 2\varsigma_{n-1} + \varsigma_n) + Q_C (\eta_{n-2} - 2\eta_{n-1} + \eta_n) \\
\frac{d\eta_n}{d\tau} &= \Pi[\varsigma_{n-1}, \varsigma_n, \varsigma_{n+1}] \cdot (\varsigma_{n-1} - 2\varsigma_n + \varsigma_{n+1}) + Q_C (\eta_{n-1} - 2\eta_n + \eta_{n+1}) \\
\frac{d\eta_{n+1}}{d\tau} &= \Pi[\varsigma_n, \varsigma_{n+1}, \varsigma_{n+2}] \cdot (\varsigma_n - 2\varsigma_{n+1} + \varsigma_{n+2}) + Q_C (\eta_n - 2\eta_{n+1} + \eta_{n+2}) \\
&\quad \vdots \\
\frac{d\eta_N}{d\tau} &= \Pi[\varsigma_{N-1}, \varsigma_N, \varsigma_L] \cdot (\varsigma_{N-1} - 2\varsigma_N + \varsigma_L) + Q_C (\eta_{N-1} - 2\eta_N + \eta_L) \\
\frac{d\eta_L}{d\tau} &= \Pi_0[\varsigma_N, \varsigma_L] \cdot (\varsigma_N - \varsigma_L) + Q_C \eta_N - (Q_L + Q_C) \eta_L
\end{aligned}$$

where

$$\begin{aligned}
\Pi[\varsigma_{n-1}, \varsigma_n, \varsigma_{n+1}] &= 1 + \Lambda (\varsigma_{n-1}^2 + \varsigma_n^2 + \varsigma_{n+1}^2 - \varsigma_{n-1}\varsigma_n - \varsigma_n\varsigma_{n+1} - \varsigma_{n+1}\varsigma_{n-1}) \\
\Pi_0[q_{n-1}, q_n] &= 1 + \Lambda (\varsigma_{n-1} - \varsigma_n)^2
\end{aligned}$$

and $\Lambda = \alpha C^3 V_S^2$ measures the system nonlinearity.

NO. OF COPIES	ORGANIZATION	NO. OF COPIES	ORGANIZATION
1 ELEC	ADMNSTR DEFNS TECHL INFO CTR ATTN DTIC OCP 8725 JOHN J KINGMAN RD STE 0944 FT BELVOIR VA 22060-6218	1 HC	COMMANDER US ARMY RDECOM ATTN AMSRD AMR W C MCCORKLE 5400 FOWLER RD REDSTONE ARSENAL AL 35898-5000
1 HC	DARPA ATTN IXO S WELBY 3701 N FAIRFAX DR ARLINGTON VA 22203-1714	1 HC	US GOVERNMENT PRINT OFF DEPOSITORY RECEIVING SECTION ATTN MAIL STOP IDAD J TATE 732 NORTH CAPITOL ST NW WASHINGTON DC 20402
1 CD	OFC OF THE SECY OF DEFNS ATTN ODDRE (R&AT) THE PENTAGON WASHINGTON DC 20301-3080	1 HC	DEPT OF PHYSICS AND GEOLOGY UNIV OF TEXAS - PAN AMERICAN ATTN S TIDROW 1201 W UNIVERSITY DR EDINBURG TX 78541
1 HC	US ARMY RSRCH DEV AND ENGRG CMND ARMAMENT RSRCH DEV & ENGRG CTR ARMAMENT ENGRG & TECHNLGY CTR ATTN AMSRD AAR AEF T J MATTS BLDG 305 ABERDEEN PROVING GROUND MD 21005-5001	1 HC	US ARMY RSRCH LAB ATTN RDRL CIM G T LANDFRIED BLDG 4600 ABERDEEN PROVING GROUND MD 21005-5066
1 HC	PM TIMS, PROFILER (MMS-P) AN/TMQ-52 ATTN B GRIFFIES BUILDING 563 FT MONMOUTH NJ 07703	25 HCS	US ARMY RSRCH LAB ATTN IMNE ALC HRR MAIL & RECORDS MGMT ATTN RDRL CIM L TECHL LIB ATTN RDRL CIM P TECHL PUB ATTN RDRL SE J PELLEGRINO ATTN RDRL SED E D KATSIS ATTN RDRL SED E S HENRIQUEZ ATTN RDRL SED M J TATUM ATTN RDRL SED P K JONES ATTN RDRL SEE I S SVENSSON ATTN RDRL SEE O W M GOLDING ATTN RDRL SER E E VIVEIROS ATTN RDRL SER E F CROWNE (5 COPIES) ATTN RDRL SER E R DEL ROSARIO ATTN RDRL SER J MAIT ATTN RDRL SER L D POTREPKA ATTN RDRL SER L J PULSKAMP ATTN RDRL SER L M DUBEY ATTN RDRL SER L R POLCAWICH ATTN RDRL SER P AMIRTHARAJ ATTN RDRL SER U C FAZI ATTN RDRL SES M PATTERSON ADELPHI MD 20783-1197
1 HC	US ARMY ARDEC ATTN AMSRD AAR AEE P C HAINES BLDG 25 PICATINNY ARSENAL NJ 07806-5000		
1 HC	US ARMY ARDEC ATTN AMSRD AAR AEM C A MARSTON BLDG 61S PICATINNY ARSENAL NJ 07806-5000		
3 HCS	US ARMY ARDEC ATTN AMSRD AAR AEM L S GILMAN ATTN AMSRD AAR AEP F O NGUYEN ATTN AMSRD AAR AEP F S SHRI BLDG 65S PICATINNY ARSENAL NJ 07806-5000		
1 HC	US ARMY INFO SYS ENGRG CMND ATTN AMSEL IE TD A RIVERA FT HUACHUCA AZ 85613-5300		
		TOTAL: 40	(1 ELEC, 1 CD, 38 HCS)